Research Article | Vol. 29, No. 5 / 1 March 2021 / Optics Express 7858
Optics EXPRESS

Tunable electrochromic filter for *in situ* Fourier spatial frequency filtering

A. Hein, B. Kaiser, C. Kortz, and E. Oesterschulze*

Technische Universität Kaiserslautern, Erwin-Schrödinger-St. 46, 67663 Kaiserslautern, Germany
**oester@rhrk.uni-kl.de*

Abstract: Spatial optical Fourier filtering is a widespread technique for *in situ* image or light field processing. However, conventional fixed absorbing patterns or mechanical irises only allow an inflexible, very restricted control. Thus, we present two electrochromic spatial filters with ring-shaped or directional segments, which can be individually addressed and continuously tuned in transmission resulting in up to 512 different filtering states. For realization of the electrochromic devices, we overcome technical obstacles to realize seamless, gap-free electrochromic segments. We describe this novel fabrication process and demonstrate the successful application in an optical Fourier transform set-up.

1. Introduction

In Fourier optics the electric field distribution of an object is described as superposition of plane waves with certain spatial frequency components k[1]. To get access to the entire object's spatial frequency distribution, a lens is typically exploited with the illuminated object in the front focal plane and the resultant Fourier transform of the object's field distribution in its back focal plane. In this so called 2f Fourier transform set-up, spatial frequency filtering is performed by blocking certain frequency components in the back focal plane. Low pass filtering is performed using a fixed or adjustable mechanical iris where the radius of the open aperture determines the maximum passing object's spatial frequency. This set-up is used for the elimination of high frequency noise of laser profiles or low pass filtering in optical image processing to name only few applications.

Recently, different active iris devices were presented in the literature to replace the bulky mechanical devices in the evolving field of microoptics. Some of them rely on concepts close to that of a classical blade iris [2,3], others on liquid displacement or electrowetting techniques [4–6]. All these filters exploit the motion of optically absorbing matter into the light path which restricts their use solely to low-pass filtering. Active filters with spatially controllable absorption like pixel oriented liquid crystal modulators can be used to extend this image processing concept also to more sophisticated spatial filtering characteristics like band-pass or high-pass filtering. However, these expensive devices are too voluminous to be integrated into microoptical devices.

Meanwhile, tunable filters were presented that exploit electrochromic (EC) materials. These materials change their appearance from colorless to colored continuously when an appropriate electric potential is applied. Homogeneously colored EC devices are already commercially available as auto-dimming mirrors or switchable windows [7]. In earlier publications we presented first solutions of miniaturized EC irises that were capable to gain spatial control [8–11]. These EC iris devices as well as other homogeneous EC filters reported in the literature benefit from their low control voltages and power uptake and additionally their low volume consumption. However, they were affected either by low contrast or long switching time constants [12–14]. One promising approach is to combine organic EC materials such as viologen with EC polymers or inorganic materials such as Prussian blue or Co_3O_4 [15–18]. This way, switching times and optical behavior can be tuned. Meanwhile, we reported on EC neutral filters based on nanoparticle layer (NPL) electrodes which were covered with monolayers of EC organic molecules [19]. Viologen molecules chemisorbed onto TiO_2 NPL and tetraphenylbenzidine (TPB) on antimony

#418048 https://doi.org/10.1364/OE.418048
Journal © 2021 Received 21 Dec 2020; revised 26 Jan 2021; accepted 26 Jan 2021; published 26 Feb 2021

Optics EXPRESS

doped tin oxide (ATO) NPL have been used as complementary materials. The combination of EC molecules with high coloration efficiency and conductive nanoparticles enabled excellent switching times of less than 1 s with at least 90 % Michelson contrast over the entire optical spectral range [19].

Using this optimized material composition, we herein present a microfabricated tunable EC iris for low pass, band pass and high pass filtering and additionally EC azimuthal sector devices for directional spatial Fourier processing. For their implementation we overcome two important technical obstacles of segmented EC devices. We avoided the insulating gap between adjacent EC segments that deteriorates imaging contrast of the devices [10] by covering the segmented transparent control electrodes by means of a homogeneous nanoparticle layer carrying the EC molecules. Concurrently, this also reduced the impact of the misalignment of the cathodic coloring (viologen/TiO_2) and anodic colouring (TPB/ATO) electrode.

2. Fabrication

In Fig. 1(a), the EC materials and the structure of the device are shown. We have left the conductive indium tinoxide (ITO) layer of the anodic electrode unstructured and used it during operation as overall counter electrode for all segments of the opposing cathodic electrode. In this way we have not only bypassed the above mentioned intricate alignment process of sub- and superstrate. In fact, this configuration proved advantageous because for small separation distances of 50 μm, the coloration on the anodic electrode follows the coloration of the cathodic

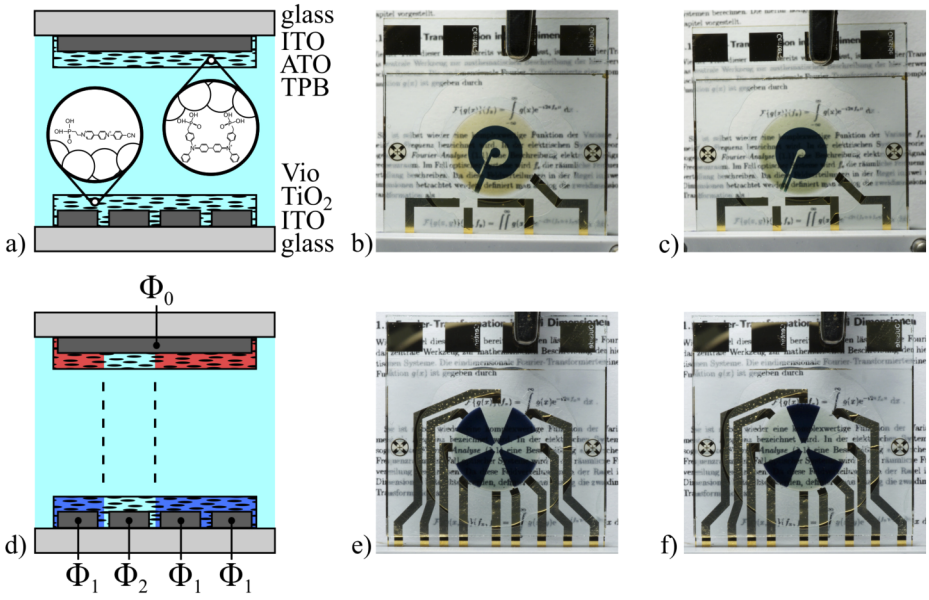

Fig. 1. a) Schematic cross section of a EC device with a structured (bottom) and unstructured ITO electrode (top) and the corresponding EC materials, b) and c) optical images of the EC iris in two different switching states, d) cross section with applied electric potentials resulting in a transfer of the coloration on the lower electrode to the upper electrode, e) and f) optical images of an azimuthally structured spatial EC filter with eight segments and an additional center electrode. In all devices, the distance between adjacent segments of the ITO layer is 50 μm. Colored segments are addressed with $\Phi_1 = -1.5$ V, transparent segments with $\Phi_2 = +1.5$ V. The optical images were taken with fixed illumination conditions (exposure time 1/13 s, ISO 640) to provide comparability.

Optics EXPRESS

electrode as shown in Fig. 1(d) [20]. This way, we can control the EC materials on both electrodes applying the indicated potentials Φ_1 and Φ_2 with respect to the reference potential $\Phi_0 = 0$ V.

Our EC filter cells were build up from two ITO coated glass substrates (8-12 Ω/sq, Sigma Aldrich) with an electrolyte (1 mol/l $LiClO_4$ in propylene carbonate) sandwiched in between. For cleaning they were first sonicated in acetone, isopropanol, and DI water for 5 min each and dried under a nitrogen stream. As shown in Fig. 2, alignment marks and contact pads made of 10 nm Cr and 90 nm Au were deposited by magnetron sputtering followed by UV lithography and etching. Thereafter, the ITO layer of the cathodic electrode was structured by UV lithography and wet etching with an aqueous solution of hydrochloric acid in such a way that defines the contour of the iris segments or segments of the directional spatial filter. We have established a four stage iris (Figs. 1(b)-(c)) as well as an azimuthally segmented filter with eight pie shaped segments plus a central electrode for the control of the low frequency components (Figs. 1(e)-(f)).

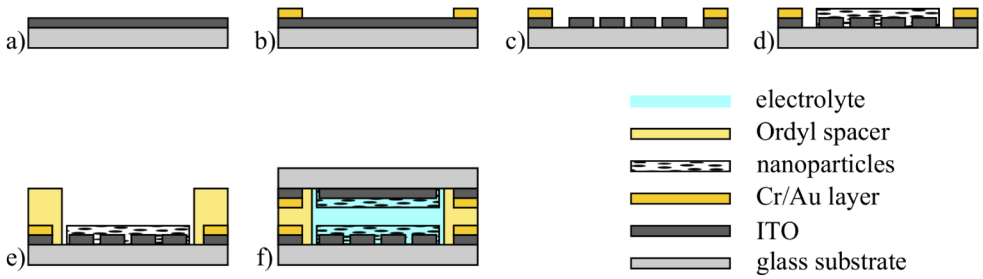

Fig. 2. Fabrication process of the EC device: a) ITO coated glass substrate, b) sample after Cr/Au deposition and structuring, c) sample after ITO structuring, d) sample with doctor-bladed and sintered nanoparticle layer, e) sample with laminated and structured Ordyl spacer layer, f) encapsulated device with functionalized nanoparticle layers after electrolyte filling and bonding. For structuring, UV-lithography and wet chemical etching was used (see [19] for details). The legend gives the color code for different materials.

In the final step before encapsulation, the TiO_2 NPL with the chemisorbed viologen molecules as well as the ATO NPL with TPB was deposited as homogeneous layers onto both the structured cathodic electrode and the unstructured anodic electrode, respectively (see [19] for details). Owing to the conductivity of both NPLs we get the desired concurrent coloring in the insulating 50 μm gap when two adjacent segments are switched (see Fig. 1(c)). To receive also a strong drop of absorption at the edge of a single switched segment, the adjacent segments were biased to their translucent state, which results in a low current of less than 0.4 mA.

3. Results and discussion

In a first step all devices were characterized with respect to their spectral as well as temporal behavior. As shown in Fig. S1 of the Supplement 1, the transmission in the cleared state is almost constant over the entire optical range. In the opaque state we receive transmission as low as 1-2 % except in the spectral range from 450 to 550 nm, which is consistent with our previous work [19]. Our EC devices provide an excellent Michelson contrast of $(T_{max} - T_{min})/(T_{max} + T_{min}) = 97.2$ % at the wavelength of a HeNe laser ($\lambda = 632.8$ nm). This laser was used for all spatial filtering experiments. Temporally resolved measurements revealed time constants for bleaching and clearing that are both well below 1 s (see Fig. S1 in Supplement 1).

The individually switchable filter elements are controlled by the segmented cathodic electrodes. The EC material on top of a negative charged electrode turns into its colored state whereas the EC material on top of a positive charged segment remains transparent. One major finding of the paper is that the coloration distribution on the unstructured anodic electrode follows the

Optics EXPRESS

coloration distribution of the cathodic electrode as can be seen in the schematic cross section and the photographs of the two devices in Fig. 1. The filter segments appear sharp and the edges of the filter segments are well defined. Another benefit from this kind of structuring is that the coloration over two segments is homogeneous if neighboring elements are colored due to the continuous NPL as demonstrated in Fig. 1(c). This ability of a homogeneous coloration is mandatory for a seamless frequency filtering process.

Spatial frequency filtering was performed in the 2f-plane of a conventional 4f Fourier filtering set-up (Fig. 3). For the illumination of the object, the beam of a He-Ne laser ($\lambda = 632.8$ nm) was expanded with a telescope set-up by a factor of 50. A 80 μm pinhole was added to eliminate high frequency noise and thus improve the TEM_{00} laser beam profile [21]. An aperture close after the telescope set-up restricted the central part of the Gaussian beam profile for the almost homogeneous illumination of the object. We used achromatic lenses ($f = 400$ mm, AC508-400-A, ThorLabs) for the 4f set-up to reduce spherical aberration during the two consecutive Fourier transform processes. For the manipulation of the object's Fourier spectrum, our EC devices were placed in the Fourier plane of lens 1 to eliminate certain spatial frequency components. By means of the second Fourier transform with lens 2 the spatially filtered image is received in the back focal plane of lens 2. While all Fourier transformations process the complex electric field E, the camera and thus our measurements show the intensity $I \propto E^* E$.

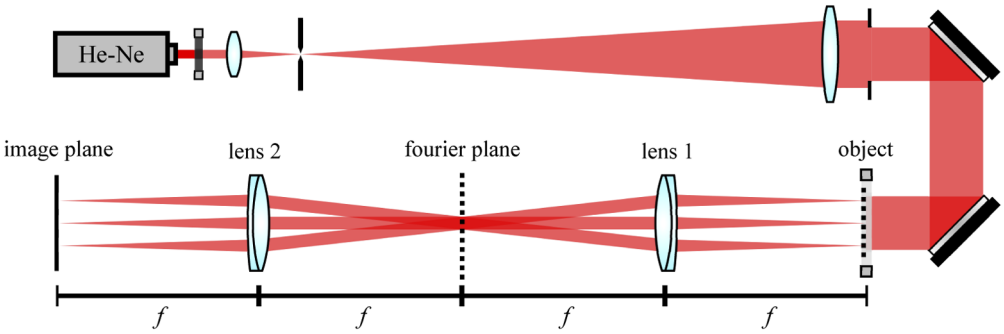

Fig. 3. Experimental set-up: The object is illuminated by an expanded beam of a HeNe laser, lenses 1 and 2 are operated in the 2f configuration to establish two consecutive Fourier transformations. The EC-filter is placed in the first Fourier plane which is the back focal plane of lens 1.

Spatial filtering was demonstrated employing a spoke target or Siemens star test target (in the following abbreviated as Siemens star) consisting of 72 pie-shaped opaque segments on a glass substrate with a 1 to 0 duty cycle of transmission along the circumference of radius r. The associated transmission profile is a periodic rectangular transmission function with a technical frequency that is inversely proportional to the radius:

$$k_0 = 72/(2\pi r). \tag{1}$$

It is measured in line pairs/mm. However, the detailed mathematical analysis of this rectangular transmission function in the object plane x in terms of a Fourier series reveals the relevant set of spatial frequencies $(2n-1)k_0$ defined in units of 1/m with amplitude $A_n \propto 1/n$:

$$T(x) = A_0 + \sum_{n=1} A_n \cos\left(2\pi(2n-1)\cdot k_0 \cdot x\right) \text{ with: } n = 1, 2, \ldots \tag{2}$$

For spatial frequency filtering the iris is centered in the so called Fourier plane that coincides with the back focal plane of the lens. If we now color a particular circular segment of the iris

Optics EXPRESS

with radius $r_{\text{colored},1}$ to $r_{\text{colored},2}$, this will block all corresponding spatial frequencies in the range $\left[r_{\text{colored},1}/(\lambda \cdot f), r_{\text{color},2}/(\lambda \cdot f)\right]$ for all directions. This means that these spatial frequencies are suppressed for every transmission profile all over the Siemens star pattern and thus removed from the spatial Fourier series. The second lens in the 4f Fourier filter arrangement produces a consecutive Fourier transformation and allows us to investigate the filtering process in the image plane.

In Fig. 4 we have demonstrated this filtering process for an iris segment covering all radii from $r_{\text{colored},1} = 0.5\,\text{mm}$ to $r_{\text{colored},2} = 1.5\,\text{mm}$, which corresponds to the spatial frequency range within $k_{\text{colored},1} = r_{\text{colored},1}/(\lambda f) = 2.0\,\text{mm}^{-1}$ and $k_{\text{colored},2} = r_{\text{colored},2}/(\lambda f) = 5.9\,\text{mm}^{-1}$. If we now extract the profile of the filtered Siemens star at radius $r_1 = 3.9\,\text{mm}$ (see Fig. 4(c)), the basic spatial frequency $k_0(r_1) = 2.9\,\text{mm}^{-1}$ (see Eq. (1)) is removed, as it falls within the suppressed frequency range. Therefore, all other Fourier components of the series remain with the leading frequency $3k_0$.

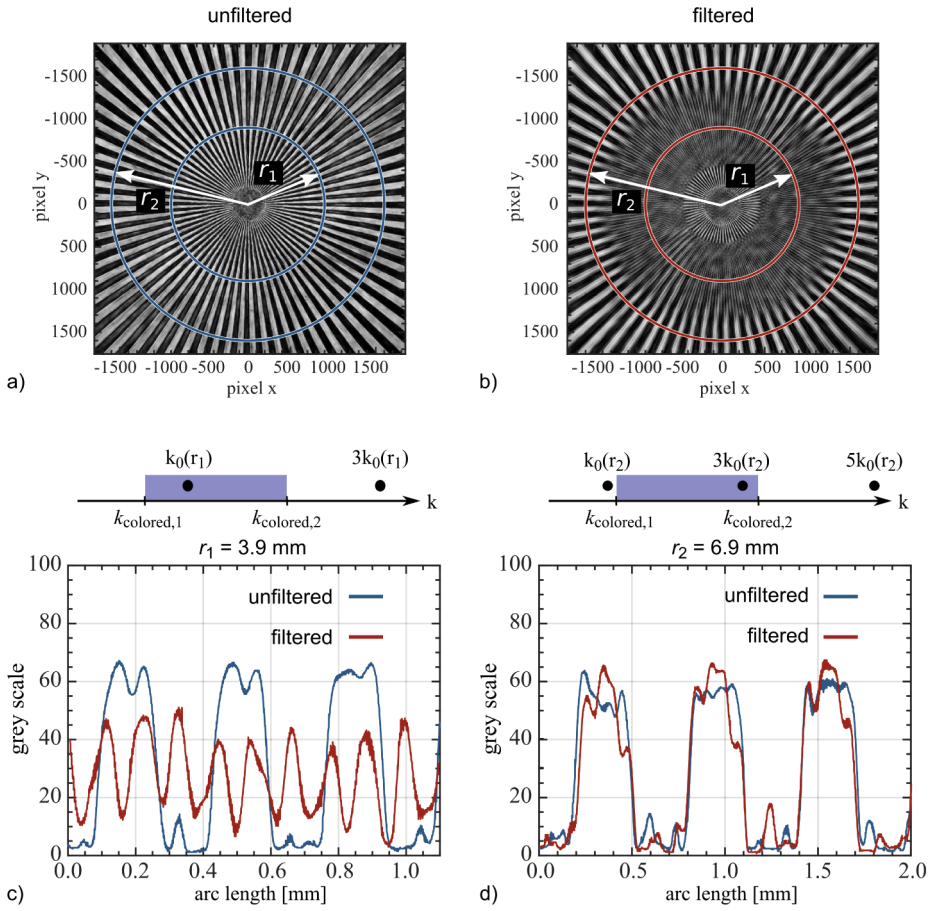

Fig. 4. Optical images of the (a) unfiltered and (b) filtered Siemens star and measured corresponding transmission profiles at the indicated radii (c, d). Both images (a) and (b) were taken in the image plane while all segments of the EC iris were switched to the transparent state in (a) and only the second segment was switched opaque in (b). The k-scale in (c) and (d) illustrates the blocked frequency range and the resulting blocked frequency components in the Fourier series at the two exemplary radii.

Optics EXPRESS

Figure 4(d) shows that at $r_2 = 6.9$ mm the leading frequency component $k_0(r_2) = 1.7\,\mathrm{mm}^{-1}$ is not affected, while in this case $3k_0$ is suppressed. In the filtered profile, this results in rounded edged of the previously rectangular-shaped signal. For the two given exemplary radii r_1 and r_2, the k-scale with the Fourier components and the blocked spatial frequency range is illustrated in Figs. 4(c) and (d).

The demonstrated optical band pass filtering is a unique feature of the EC iris. Conventional mechanical irises only allow low pass filtering by moving the blades into the path of light. However, to study the effect of the limited Michelson contrast of our device, we used lithographic processes to fabricate 150 nm thick Cr masks on glass substrates with ring-shaped patterns according to the rings of the EC iris. In Fig. S2 in the Supplement 1, we apply several static Cr masks and adjustable EC iris filter states and compare the Siemens star images. The results show high accordance and thus confirm the good optical image quality of the EC Filter. While we had to fabricate multiple Cr masks for this experiment and manually install and remove every single one for each measurement, the EC iris conveniently combines all these filter characteristics in a single device.

The directionally controlled filtering was demonstrated using a diffraction object in form of a modified version of the TU Kaiserslautern logo; the 'Gate of Science'. It consists of 4 segments: a left and right column and two parts of the roof. Each segment consists of a line pattern with 5 line pairs per millimeter. The grids are rotated by an angle of 45° for the different segments of the 'gate' thus every part of the image gives a characteristic pattern in the Fourier plane which are distinguishable from each other (see color code pattern in Fig. 5(a)). Using a filter like the one displayed in Figs. 1(e)-(f) each segment of the gate can be individually addressed. The results are shown in Fig. 5 where the upper images show the intensity pattern in the Fourier plane and the EC-filter in different switching states. The lower images show the 'Gate of Science' in the image-plane manipulated with the EC-filter in the above demonstrated switching state. Suppressed segments disappear almost completely in the filtered image, as the pie-shaped filter elements eliminate all directional frequency components and the center segment is switched opaque, as well. Considering that each of the 9 segments can be switched transparent or opaque, $2^9 = 512$ different filter states are possible.

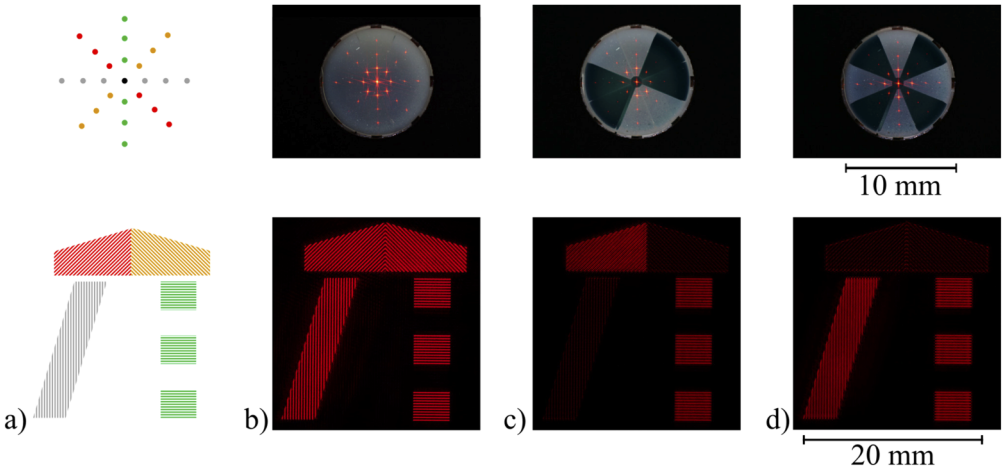

Fig. 5. a) Schematic Fourier pattern (top) of the 'Gate of Science' (bottom) with correlated directional spatial frequency components in color code, (b - d) optical images of different switching states in the Fourier plane (top) and image plane (bottom). The patterns have 5 line pairs / mm.

Optics EXPRESS

Additionally, the transmission of an EC device can not only be switched from on to off, it can also be tuned in transmission which we have used for a graduated filter before [20,22]. In electrochemical cells, the Nernst equation states the concentration of oxidized (i.e. transparent) and reduced (i.e. colored) molecules is dependent on the applied electric potential which explains the sigmoidal transmission-potential dependence [20]. In Fig. S3 in the Supplement 1 we demonstrate that by applying intermediate potentials of −0.6 V or −1.0 V, the transmission of each segment of the EC iris can be individually tuned, enabling continuous space frequency filtering. Moreover, a video of the fast response of the device and its effect on the image in real time is attached (see Visualization 1).

4. Conclusion

By combining micro fabrication processes with a fast, high contrast EC material system, we were able to realize a tunable spatial frequency as well as directional dependent spatial frequency filter. We have shown a fabrication method for an EC device which allows individual tuning of gap-less segments. By structuring only the conductive ITO layer on one of the electrodes, we faciliated the microoptical device fabrication and kept the EC layers homogeneous. Therefore, the optical quality and performance of the EC iris in the Fourier plane was comparable to conventional mechanical irises and even allowed additional filter characteristics such as optical bandpass filtering. The resulting effects thereof were discussed and explained for an exemplary Siemens star object. Furthermore, directional Fourier filtering was demonstrated, showing that periodic structures in an image can be precisely suppressed. The presented EC filter elements combine up to 512 different filter characteristics in one device if only operated in the on/off mode. Moreover, they offer convenient tunability with voltages in the range of ±2 V. This proofs that they are ideally suitable for the implementation into optical systems for *in situ* space frequency filtering.

Funding. Deutsche Forschungsgemeinschaft (EO220/19-1).

Acknowledgements. We thank the national research foundation (DFG) for their financial support under contract number EO220/19-1 and the Nano Structuring Center (NSC) Kaiserslautern for their technical support.

Disclosures. The authors declare no conflicts of interest.

Supplemental document. See Supplement 1 for supporting content.

References

1. J. W. Goodman, *Introduction to Fourier Optics* (WH Freeman, 2017), 4th ed.
2. G. Zhou, H. Yu, Y. Du, and F. S. Chau, "Microelectromechanical-systems-driven two-layer rotary-blade-based adjustable iris diaphragm," Opt. Lett. **37**(10), 1745–1747 (2012).
3. Y. Hongbin, Z. Guangya, D. Yu, M. Xiaojing, and S. C. Fook, "MEMS-Based Tunable Iris Diaphragm," J. Microelectromech. Syst. **21**(5), 1136–1145 (2012).
4. P. Müller, N. Spengler, H. Zappe, and W. Mönch, "An optofluidic concept for a tunable micro-iris," J. Microelectromech. Syst. **19**(6), 1477–1484 (2010).
5. S. Petsch, S. Schuhladen, L. Dreesen, and H. Zappe, "The engineered eyeball, a tunable imaging system using soft-matter micro-optics," Light: Sci. Appl. **5**(7), e16068 (2016).
6. P. Müller, R. Feuerstein, and H. Zappe, "Integrated Optofluidic Iris," J. Microelectromech. Syst. **21**(5), 1156–1164 (2012).
7. P. M. S. Monk, D. R. Rosseinsky, and R. J. Mortimer, *Electrochromic Materials and Devices* (Wiley-VHC, 2015).
8. T. Deutschmann and E. Oesterschulze, "Micro-structured electrochromic device based on poly(3, 4-ethylenedioxythiophene)," J. Micromech. Microeng. **23**(6), 065032 (2013).
9. T. Deutschmann and E. Oesterschulze, "Integrated electrochromic iris device for low power and space-limited applications," J. Opt. **16**(7), 075301 (2014).
10. D. Pätz, T. Deutschmann, E. Oesterschulze, and S. Sinzinger, "Depth of focus analysis of optical systems using tunable aperture stops with a moderate level of absorption," Appl. Opt. **53**(28), 6508–6512 (2014).
11. T. Deutschmann, C. Kortz, L. Walder, and E. Oesterschulze, "High contrast electrochromic iris," Opt. Express **23**(24), 31544–31549 (2015).
12. F. Campus, P. Bonhote, M. Grätzel, S. Heinen, and L. Walder, "Electrochromic devices based on surface-modified nanocrystalline TiO_2 thin-film electrodes," Sol. Energy Mater. Sol. Cells **56**(3-4), 281–297 (1999).
13. P. Bonhote, E. Gogniat, F. Campus, L. Walder, and M. Grätzel, "Nanocrystalline electrochromic displays," Displays **20**(3), 137–144 (1999).

Optics EXPRESS

14. M. Möller, S. Asaftei, D. Corr, M. Ryan, and L. Walder, "Switchable Electrochromic Images Based on a Combined Top-Down Bottom-Up Approach," Adv. Mater. **16**(17), 1558–1562 (2004).
15. A. Chaudhary, D. Pathak, S. Mishra, P. Yogi, P. Sagdeo, and R. Kumar, "Enhancing Viologen's Electrochromism by Incorporating Thiophene: A Step Toward All-Organic Flexible Device," Phys. Status Solidi A **216**(2), 1800680 (2018).
16. A. Chaudhary, D. Pathak, M. Tanwar, P. Sagdeo, and R. Kumar, "Prussian Blue-Viologen Inorganic-Organic Hybrid Blend for Improved Electrochromic Performance," ACS Appl. Electron. Mater. **1**(6), 892–899 (2019).
17. A. Chaudhary, D. Pathak, T. Ghosh, S. Kandpal, M. Tanwar, C. Rani, and R. Kumar, "Prussian Blue-Cobalt Oxide Double Layer for Efficient All-Inorganic Multicolor Electrochromic Device," ACS Appl. Electron. Mater. **2**(6), 1768–1773 (2020).
18. D. Pathak, A. Chaudhary, M. Tanwar, U. Goutam, and R. Kumar, "Nano-cobalt oxide/viologen hybrid solid state device: electrochromism beyond chemical cell," Appl. Phys. Lett. **116**(14), 141901 (2020).
19. C. Kortz, A. Hein, M. Ciobanu, L. Walder, and E. Oesterschulze, "Complementary hybrid electrodes for high contrast electrochromic devices with fast response," Nat. Commun. **10**(1), 4874 (2019).
20. A. Hein, C. Kortz, and E. Oesterschulze, "Tunable graduated filters based on electrochromic materials for spatial image control," Sci. Rep. **9**(1), 15822 (2019).
21. E. Hecht, *Optics* (Addison Wesley, 2002), 4th ed.
22. A. Hein, N. Longen, C. Kortz, F. Carl, J. Klein, M. Haase, and E. Oesterschulze, "Two-dimensional spatial image control using an electrochromic graduated filter with multiple electrode configuration," Sol. Energy Mater. Sol. Cells **10**, 4874 (2020).